Design and Cascade PI Controller-Based Robust Model Reference Adaptive Control of DC-DC Boost Converter

CAGFER YANARATES AND **ZHONGFU ZHOU**

Electrical and Electronic Engineering Department, Swansea University, Swansea SA1 8EN, U.K.

Corresponding author: Cagfer Yanarates (cagferyanarates@gmail.com)

ABSTRACT In this paper, Cascade PI Controller-Based Robust Model Reference Adaptive Control (MRAC) of a DC-DC boost converter is presented. Non-minimum phase behaviour of the boost converter due to right half plane zero constitutes a challenge and its non-linear dynamics complicate the control process while operating in continuous conduction mode (CCM). The proposed control scheme efficiently resolved complications and challenges by using features of cascade PI control loop in combination with properties of MRAC. The accuracy of the proposed control system's ability to track the desired signals and regulate the plant process variables in the most beneficial and optimised way without delay and overshoot is verified using MATLAB/Simulink by applying comparative analysis with single PI and cascade PI controllers. Moreover, performance of the proposed control scheme is validated experimentally with the implementation of MATLAB/Simulink/Stateflow on dSPACE Real-time-interface (RTI) 1007 processor, DS2004 High-Speed A/D and CP4002 Timing and Digital I/O boards. The experimental results and analysis reveal that the proposed control strategy enhanced the tracking speed two times with considerably improved disturbance rejection.

INDEX TERMS Cascade PI controller, control systems mathematical models, model reference adaptive control, state-space averaging method, time and frequency domain analysis.

I. INTRODUCTION

Growing global energy consumption, as well as issues of shortage and environmental effects connected with conventional energy sources, are putting the world on the verge of an energy catastrophe in the next two or three decades [1]–[3]. The energy problem linking between energy access and greenhouse gas emissions has been given more attention recently, and consequently there has been a noticeable increase in the use of renewable energy sources for power generation around the world [4]–[6].

Because of inconsistent power generation from sustainable energy sources, which is dependent on the environment, they are difficult to utilise without switching power supply, including the power conditioner. According to the statistics in [7]–[9] the vast majority of electricity generated in developed countries, i.e. over 90% of generated power,

is handled by power electronic circuits before being transmitted to the utility [10]–[12]. As a result, switching power supply energy efficiency (environmental protection), footprints (smart packaging technologies), power density (to reduce weight/volume) and reliability to achieve zero defect design for components and systems is critical in the renewable energy system applications [13]–[15].

Switched-mode power supplies (also known as a switched-mode power supply, switched power supply, SMPS, or switcher) are electronic power supplies that include switching regulators to efficiently convert electrical power. While converting voltage and current characteristics, an SMPS, like other power supplies, transforms power from a DC or AC source to DC loads. Because the switching transistor dissipates less power when serving as a switch, SMPS has a high efficiency up to 96 percent [16], [17]. Other benefits include reduced size, noise, and weight due to the absence of heavy line-frequency transformers, as well as reduced heat generation [18], [19]. The circuit topology of the SMPS can

The associate editor coordinating the review of this manuscript and approving it for publication was Jinquan Xu.

TABLE 1. The fundamental forms of non-isolated converters.

Type	Typical Power (W)	Energy Storage	Voltage Relation	Features
Buck Converter	0-1,000	Single Inductor	$0 \leq V_{out} \leq V_{in}$ $V_{out} = DV_{in}$	Continuous current at output
Boost Converter	0-5,000	Single Inductor	$V_{out} \geq V_{in}$ $V_{out} = \dfrac{1}{1-D}V_{in}$	Continuous current at input
Buck-boost Converter	0-150	Single Inductor	$V_{out} \leq 0$ $V_{out} = -\dfrac{D}{1-D}V_{in}$	Discontinuous current at both input and output

FIGURE 1. The magnitude and phase plot from duty cycle to load voltage on the intended frequency range.

be used to classify them. The most significant distinctions to consider are isolated and non-isolated converters [20]–[22].

The three fundamental forms of non-isolated converters all use a single inductor for energy storage given in Table 1. D is the duty cycle of the converter in the voltage relation column, and it can range from 0 to 1. The input voltage (V_{in}) is expected to be larger than zero; if it is negative, negate the output voltage for consistency's sake (V_{out}).

The DC-DC boost converter (DBC) is the simplest converter topology for effectively reproducing increased output voltage for a given input voltage [23]. It has been used in a wide range of applications such as automotive industry (hybrid electric vehicles), power amplifications, adaptive control applications, battery power systems, consumer electronics, robotics, DC motor drives, communication applications (radar systems), wind power and photovoltaic (PV) systems (e.g., DC micro-grid) [24]–[26].

Because of exhibiting non-minimum phase (NMP) behaviour due to right half plane zero (RHPZ) and non-linear dynamics, controller design for DBCs is more complex and challenging than for buck converters [27]–[29]. The comparative analysis of the most common developed control techniques for SMPS applications in terms of their features, advantages, and limitations is given in Table 2. The phenomenon commonly known as the NMP behaviour is the phase lag caused by transfer of accumulated energy of the inductor when the switch is on to the load during off time. This attribute is reflected by the existence of a RHPZ in the control to output voltage transfer function [26]. By restricting the closed loop bandwidth feasible by feedback control, the NMP nature complicates the control effort. The dynamic change in positive zero location induced by varying converter settings such as load resistance and voltage gain exacerbate the NMP problem. Moreover, a reduction in input voltage or load resistance tends to destabilise the closed loop system by shifting the RHPZ towards origin.

The following two categories can be used to categorise the methods offered in the literature to address the NMP problem in a DBC: (i) converter topology modification approaches to achieve minimum phase (MP) dynamics. (ii) specially built controllers that correct for NMP dynamics. In this study, the second strategy is used by utilizing the properties of both cascade PI controller and reference model adaptive control
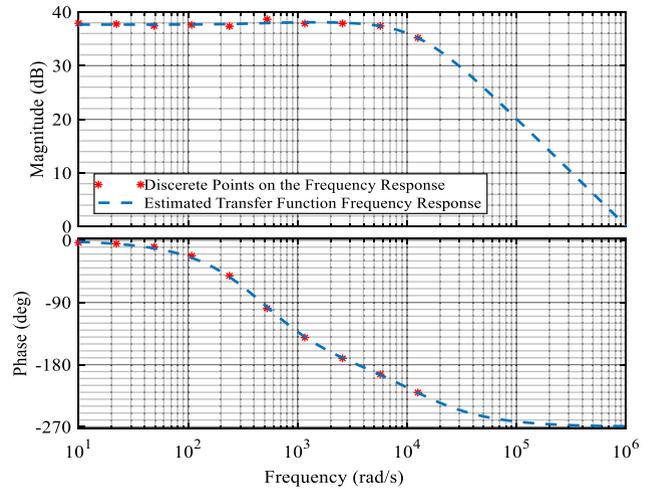
in consideration of the inherent challenges, such as non-linearity, NMP nature, time discontinuities, and model uncertainty (unknown parasitic values, resistance and voltage drops across switching element and diode, uncertainty in the value of inductance etc.).

The remainder of the paper is structured out as follows. Section II. presents transfer function estimation of the designed hardware of the DBC in CCM by using computer aided and state-space averaging transfer function estimation methods including step and frequency response comparison for the verification of modelling. Section III. introduces commonly used mathematical modelling techniques and presents a comparison analysis of them. Section IV. gives wide coverage to design of single PI, cascade PI, cascade PI-based model reference adaptive controllers and reference model designing together with discretization process of the derived transfer functions. The simulation and experimental results are displayed in Section V. for varying conditions to validate the enhanced performance of the proposed cascade PI-based model reference adaptive control scheme for the designed DBC. The paper ends with conclusions in Section VI.

II. TRANSFER FUNCTION ESTIMATION OF THE BOOST CONVERTER

A. COMPUTER AIDED TRANSFER FUNCTION ESTIMATION
Transfer function of the boost converter is derived by using Simulink® Control Design™. The transfer function estimation process is based on collecting frequency response data from the Simulink model of the proposed converter whose parameters are given in Table 3.

Transfer function of a boost converter can be modelled using the relationship of various interacting parameters of the device. In this paper, transfer function from the PWM duty cycle set-point to the load voltage is the subject of the study to be interested and designing controllers depends on this association. Collecting frequency response data is

TABLE 2. Comparative analysis of the most common control techniques for SMPS applications.

Control Technique	Features	Advanategs	Limitations	References
Proportional-Integral (PI)	•Suitable for linear control •Low-complexity	•Simple implementation •Fast transient response •Easy integration with various control techniques	•Incapable of responding to external distubance (e.g., load variations) •High settling time, steady-state error, overshoots	[30],[31],[32],[33], [34]
Sliding Mode Control (SMC)	•Robust and suitable for non-linear control •Converge towards sliding surface	•Simple Implementation •Capable of responding to external disturbance •Fast dynamics (e.g., settling time) •Robust	•Chattering issues due to discontinuous control law •Excessive overshoots	[31],[34],[35],[36], [37],[38]
Model Predictive Control (MPC)	•Easy for online iteration •Robust and suitable for non-linear control •Eanble to predict furure states	•Enhanced transient performance with external constraints •Fast response •Efficient tracking with estimation-based techniques	•Sensitive to circuit parameters •High computational burden •Required for detailed knowledge of the model	[30],[34],[39],[40], [41]
State-space Modeling (SSM)	•Robust and suitable for non-linear control •Suitable for multiple-input and multiple-output systems •Enable to estimate plant states continuously	•Improved transient response •Less overshoot during load varying conditions	•Required for longer period of time for initial implemntation •Required for detailed knowledge of the model	[34],[42],[43],[44], [45]
Fuzzy Logic Control (FLC)	•Robust and suitable for non-linear control •Providing stability in the presence of large variations •Suitable for the systems presenting imprecise boundary conditons	•Less overshoots •Efficient tracking response •Do not require the mathematical of the plant	•High computational burden •Required for propserly defined rules for operation •Longer settling time	[34],[46],[47],[48], [49]

TABLE 3. Design parameters of the boost converter.

Parameter	Value
Input voltage(V_{dc})	20 V
Switching frequency (f_{sw})	20 kHz
Inductance (L)	100 µH
Output capacitance (C_{out})	440 µF
Constant voltage load (V_{out})	40 V
Resistance (R)	16 Ω

FIGURE 2. The depiction of state-space structure for linear time invariant systems in general.

executed by adding perturbation to the duty cycle set-point with sinusoids of different frequencies and storing the load voltage accordingly. Carried out frequency is in the range of 10 to $1/10^{th}$ rad/s of the switching frequency. The main purpose of this implementation is to figure out how the system modifies the magnitude and phase of the injected sinusoidal signals. Alternatively stated, frequency input point is the duty cycle, and the output is the load voltage. The sinusoids injected at the input point is chosen as 0.03 which is the perturbation of the operating duty cycle in the steady state which is calculated as:

$$\frac{V_{out}}{V_{dc}} = \frac{1}{1-D} \implies D = 0.5 \qquad (1)$$

The magnitude and phase plot from duty cycle to load voltage in terms of discrete points on the intended frequency range is given in Figure 1.

The Bode plot of the proposed boost converter in Figure 1. shows that the magnitude is 38 dB. There is inconsiderable resonance around 2670 rad/s and a high frequency roll-off of

around 20 dB/decade. According to these collected discrete frequency points, transfer function of the proposed boost converter is estimated as:

$$G_{boost}(s) = \frac{V_{out}(s)}{d(s)} = \frac{-1.018e06s + 4.821e08}{s^2 + 1.302e04s + 6.307e06} \qquad (2)$$

B. STATE-SPACE AVERAGING METHOD TRANSFER FUNCTION ESTIMATION

One of the developed ways for obtaining the plant's transfer function and analysing the features and behaviours of switch mode power supplies is state space averaging method [50], [59]. The approach has shown to be a very useful and convenient tool in the applications of power electronics devices due to its great understanding and ease of derivation and implementation [51], [52]. The most general state-space representation of a system with *p* inputs, *q* outputs and *n* state variables is given in Figure 2.
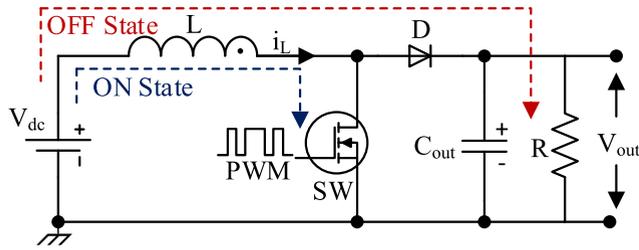
FIGURE 3. The block diagram of a boost converter.

TABLE 4. Circuit analysis of the DBC in on-off states.

where $x(.)$, $y(.)$, $u(.)$, $A(.)$, $B(.)$, $C(.)$ and $D(.)$ are state vector with $x(t) \in \mathbb{R}^n$, output vector with $y(t) \in \mathbb{R}^q$, input (control) vector with $u(t) \in \mathbb{R}^p$, state (system) matrix with $dim[A(.)] = n \times n$, input matrix with $dim[B(.)] = n \times p$, output matrix with $dim[C(.)] = q \times n$ and feedthrough (feedforward) matrix with $dim[D(.)] = q \times p$, respectively.

Block diagram of a boost converter is given in Figure 3.

Depending on the state of switch SW, the DBC has two current paths which is defined as ON and OFF operating states. Accordingly, the circuit analysis will be performed in two topologies. Circuit analysis of the DBC in both states is given in Table 4.

where V_{dc}, L, i_L, i_C, C, V_C, R, V_{out}, V_{out}/R are input DC voltage, inductance, inductor current, capacitor current, capacitance, capacitor voltage, resistive load, output voltage and output current, respectively. The vector block diagram representation of the DBC linear state-space equations is given in Figure 4.

Internal state variables are the smallest subset of system variables that can accurately describe the system's overall state at any given time. The number of state variables in
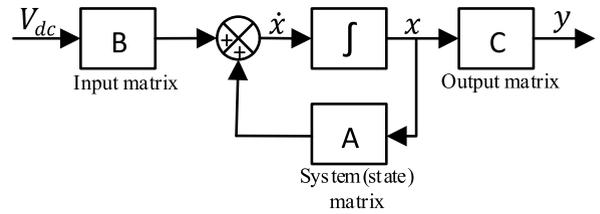
FIGURE 4. State-space vector diagram of a linear system.

electric circuits is frequently, but not always, the same as the number of energy storage devices in the circuit, such as capacitors and inductors. Accordingly, current flowing through the inductor i_L and voltage across the capacitor V_C are the state variables since the proposed boost converter consist of one inductor and one capacitor. State vector of the system is written as:

$$x = \begin{bmatrix} x_1 \\ x_2 \end{bmatrix} = \begin{bmatrix} i_L \\ V_C \end{bmatrix} \tag{3}$$

The state-space equations of the proposed boost converter are written as:

$$\dot{x} = \frac{dx}{dt} = \begin{bmatrix} \dfrac{di_L}{dt} \\ \dfrac{dV_C}{dt} \end{bmatrix} = Ax + BV_{dc}$$

$$y = V_{out} = Cx \tag{4}$$

Table 5. shows the analysis of the DBC in CCM and the derivation of its averaged state-space equation.

Averaging of the state-space model is carried out by combining ON and OFF set of equations as:

$$\dot{x} = [A_1 D + A_2(1-D)][x] + [B_1 D + B_2(1-D)]V_{dc}$$
$$V_{out} = [C_1 D + C_2(1-D)][x] \tag{5}$$

Averaged system (A), input (B) and output (C) matrices are derived by using steady-state duty cycle D as:

$$A = [A_1 D + A_2(1-D)] \Rightarrow$$
$$A = \begin{bmatrix} 0 & 0 \\ 0 & \dfrac{-1}{RC_{out}} \end{bmatrix} D + \begin{bmatrix} 0 & \dfrac{-1}{L} \\ \dfrac{1}{C_{out}} & \dfrac{-1}{RC_{out}} \end{bmatrix} (1-D) \tag{6}$$

$$A = \begin{bmatrix} 0 & 0 \\ 0 & \dfrac{-D}{RC_{out}} \end{bmatrix} + \begin{bmatrix} 0 & \dfrac{(D-1)}{L} \\ \dfrac{(1-D)}{C_{out}} & \dfrac{(D-1)}{RC_{out}} \end{bmatrix} \Rightarrow$$

$$A = \begin{bmatrix} 0 & \dfrac{(D-1)}{L} \\ \dfrac{(1-D)}{C_{out}} & \dfrac{-1}{RC_{out}} \end{bmatrix} \tag{7}$$

$$B = [B_1 D + B_2(1-D)] \Rightarrow B = \begin{bmatrix} \dfrac{1}{L} \\ 0 \end{bmatrix} D + \begin{bmatrix} \dfrac{1}{L} \\ 0 \end{bmatrix} (1-D) \tag{8}$$

$$B = \begin{bmatrix} \dfrac{D}{L} \\ 0 \end{bmatrix} + \begin{bmatrix} \dfrac{(1-D)}{L} \\ 0 \end{bmatrix} = \begin{bmatrix} \dfrac{1}{L} \\ 0 \end{bmatrix} \tag{9}$$

TABLE 5. Derivation of averaged state-space equation for the DBC in CCM.

[**State 1**: **SW ON, D OFF**] (Time interval: $0<t<dT_s$)
$\dot{x} = A_1 x + B_1 V_{dc}$
$y_1 = C_1 x$
$A_1 = \begin{bmatrix} 0 & 0 \\ 0 & \frac{-1}{RC_{out}} \end{bmatrix}$; $B_1 = \begin{bmatrix} \frac{1}{L} \\ 0 \end{bmatrix}$; $C_1 = \begin{bmatrix} 0 & 1 \end{bmatrix}$
$\begin{bmatrix} \dot{x}_1 \\ \dot{x}_2 \end{bmatrix} = \begin{bmatrix} 0 & 0 \\ 0 & \frac{-1}{RC_{out}} \end{bmatrix} \begin{bmatrix} x_1 \\ x_2 \end{bmatrix} + \begin{bmatrix} \frac{1}{L} \\ 0 \end{bmatrix} V_{dc}$
$V_{out} = \begin{bmatrix} 0 & 1 \end{bmatrix} \begin{bmatrix} x_1 \\ x_2 \end{bmatrix}$
[**State 2**: **SW OFF, D ON**] (Time interval: $dT_s<t<T_s$)
$\dot{x} = A_2 x + B_2 V_{dc}$
$y_2 = C_2 x$
$A_2 = \begin{bmatrix} 0 & \frac{-1}{L} \\ \frac{1}{C_{out}} & \frac{-1}{RC_{out}} \end{bmatrix}$; $B_2 = \begin{bmatrix} \frac{1}{L} \\ 0 \end{bmatrix}$; $C_2 = \begin{bmatrix} 0 & 1 \end{bmatrix}$
$\begin{bmatrix} \dot{x}_1 \\ \dot{x}_2 \end{bmatrix} = \begin{bmatrix} 0 & \frac{-1}{L} \\ \frac{1}{C_{out}} & \frac{-1}{RC_{out}} \end{bmatrix} \begin{bmatrix} x_1 \\ x_2 \end{bmatrix} + \begin{bmatrix} \frac{1}{L} \\ 0 \end{bmatrix} V_{dc}$
$V_{out} = \begin{bmatrix} 0 & 1 \end{bmatrix} \begin{bmatrix} x_1 \\ x_2 \end{bmatrix}$

$$C = [C_1 D + C_2 (1 - D)] \Rightarrow$$
$$C = \begin{bmatrix} 0 & 1 \end{bmatrix} D + \begin{bmatrix} 0 & 1 \end{bmatrix}(1 - D) \tag{10}$$
$$C = \begin{bmatrix} 0 & D \end{bmatrix} + \begin{bmatrix} 0 & (1-D) \end{bmatrix} = \begin{bmatrix} 0 & 1 \end{bmatrix} \tag{11}$$

The equation for steady-state operating point is written as:

$$\dot{x} = AX + BV_{dc} = 0 \tag{12}$$
$$AX = -BV_{dc} \tag{13}$$
$$A^{-1}(AX) = A^{-1}(-BV_{dc}) \Rightarrow X = A^{-1}(-BV_{dc}) \tag{14}$$

$$A^{-1} = \frac{adj(A)}{\det(A)} \Rightarrow adj(A) = \begin{bmatrix} \frac{-1}{RC_{out}} & \frac{(1-D)}{L} \\ \frac{(D-1)}{C_{out}} & 0 \end{bmatrix}$$

$$\det(A) = 0 - \left(\frac{1-D}{C_{out}} \times \frac{D-1}{L} \right) = \frac{(D-1)^2}{C_{out}L} \tag{15}$$

$$A^{-1} = \frac{1}{\frac{(D-1)^2}{C_{out}L}} \times \begin{bmatrix} \frac{-1}{RC_{out}} & \frac{(1-D)}{L} \\ \frac{(D-1)}{C_{out}} & 0 \end{bmatrix} \Rightarrow$$

$$A^{-1} = \begin{bmatrix} \frac{-L}{(D-1)^2 R} & \frac{-C_{out}}{(D-1)} \\ \frac{L}{(D-1)} & 0 \end{bmatrix} \tag{16}$$

$$B = \begin{bmatrix} \frac{1}{L} \\ 0 \end{bmatrix} \Rightarrow BV_{dc} = \begin{bmatrix} \frac{V_{dc}}{L} \\ 0 \end{bmatrix} \tag{17}$$

$$X = \begin{bmatrix} i_L \\ V_C \end{bmatrix}$$

$$= \begin{bmatrix} \frac{-L}{(D-1)^2 R} & \frac{-C_{out}}{(D-1)} \\ \frac{L}{(D-1)} & 0 \end{bmatrix} \begin{bmatrix} \frac{-V_{dc}}{L} \\ 0 \end{bmatrix} \Rightarrow$$

$$X = \begin{bmatrix} \frac{V_{dc}}{(D-1)^2 R} \\ \frac{-V_{dc}}{(D-1)} \end{bmatrix} \tag{18}$$

Small signal variations with the steady-state values are represented as:

$$d = D + \hat{d}; \quad x = X + \hat{x}; \quad y = Y + \hat{y}; \quad v_{dc} = V_{dc} + \hat{v}_{dc} \tag{19}$$

where the capitalized quantities represent the steady-state values, and the carets are small perturbations. The state-space and output equations included the perturbations are written as:

$$\dot{x} + \dot{\hat{x}} = \left[A_1 \left(D + \hat{d} \right) + A_2 \left(1 - D - \hat{d} \right) \right] [x + \hat{x}]$$
$$+ \left[B_1 \left(D + \hat{d} \right) + B_2(1 - D - \hat{d}) \right] [V_{dc} + \hat{v}_{dc}] \tag{20}$$

$$V_{dc} + \hat{v}_{dc} = \left[C_1 \left(D + \hat{d} \right) + C_2(1 - D - \hat{d}) \right] [x + \hat{x}] \tag{21}$$

Discarding the second order small signal variations in Equation(previous) results in AC small signal (dynamic) model of the system as the following:

$$\dot{\hat{x}} = A\hat{x} + [(A_1 - A_2) X + (B_1 - B_2)V_{dc}] \hat{d} \tag{22}$$
$$\hat{y} = C\hat{x} + (C_1 - C_2)X\hat{d} \tag{23}$$

The simplified representation of the state equation in Eq. 22 can be written as:

$$\dot{\hat{x}} = A\hat{x} + F\hat{d} \tag{24}$$

Variations of state variables to the duty factor can be easily solved by applying Laplace Transforms as the following:

$$\frac{\hat{x}}{\hat{d}} = [sI - A]^{-1} F \tag{25}$$

where notation I denotes the unit matrix which is the same size as the averaged system matrix A and $[sI - A]^{-1}$ is the inverse of the matrix $[sI - A]$. Converting from state-space to transfer function is performed as the followings:

$$sx(s) = Ax(s) + [(A_1 - A_2) X + (B_1 - B_2) V_{dc}] d(s) \tag{26}$$
$$V_{out}(s) = Cx(s) + [(C_1 - C_2) X] d(s) \tag{27}$$
$$x(s) = (sI - A)^{-1} [(A_1 - A_2) X + (B_1 - B_2) V_{dc}] d(s) \tag{28}$$
$$V_{out}(s) = C[(sI - A)^{-1} [(A_1 - A_2) X + (B_1 - B_2) V_{dc}] d(s)]$$
$$+ [(C_1 - C_2) X] d(s) \tag{29}$$
$$\frac{V_{out}(s)}{d(s)} = C[(sI - A)^{-1} [(A_1 - A_2) X + (B_1 - B_2) V_{dc}]$$
$$+ [(C_1 - C_2) X] \tag{30}$$

TABLE 6. Open-loop step response characteristics of derived transfer functions.

Step Response Characteristics	Simulink® Control Design™	State-space Averaging Method
Rise Time	0.0044	0.0042
Settling Time	0.0081	0.0078
Settling Minimum	68.8104	72.0324
Settling Maximum	76.4336	79.9377
Overshoot	0	0
Undershoot	85.1766	81.2702
Peak	76.4336	79.9377
Peak Time	0.0305	0.0151

$$= \frac{-sLV_{dc}+RV_{dc}(D-1)^2}{s^2\left[LRC_{out}(D-1)^2\right]+s\left[L(D-1)^2\right]+R(1-D)^4} \quad (31)$$

$$= \frac{\left(\frac{-V_{dc}}{RC_{out}(D-1)^2}\right)s+\frac{V_{dc}}{C_{out}L}}{s^2+\left(\frac{1}{RC_{out}}\right)s+\frac{(D-1)^2}{C_{out}L}}$$

$$= \frac{-0.002s+1}{2.2e-09s^2+2.5e-05s+0.0125} \quad (32)$$

Step response characteristics of the proposed boost converter transfer functions derived by using Simulink® Control Design™ and state-space averaging techniques in terms of open-loop is given in Table 6.

Open-loop step, phase and magnitude responses of the transfer functions are given in Figure 5.

III. COMPARISON OF COMMONLY USED MATHEMTICAL MODELLING TECHNIQUES

A mathematical model is a set of mathematical equations that are used to describe control systems. These models are useful for control system analysis and design. While analysis of a control system means finding the output by utilizing the input and the mathematical model of the system, designing of a control system refers to determining of the mathematical model by using the input and output of the system. Commonly used mathematical models are differential equation model, transfer function model and block diagram model. Figure 3. shows the block diagram of the proposed boost converter and the transfer function model has been derived by using both Simulink® Control Design™ and state-space averaging technique. The differential equation model is given in Figure 6.

Open-loop simulation output voltages of three mathematical models of the proposed boost converter are given in Figure 7. The figure shows that differential equation and transfer function models' transient responses resemble each other but differential equation model has a steady-state error. However, block diagram model exhibits better transient response with a steady-state error.

IV. CONTROLLER AND REFERENCE MODEL DESIGN

Due to the boost converter's intrinsic RHPZ, a voltage-mode controlled boost converter operating in CCM is more difficult to stabilize compared to other DC switch mode power
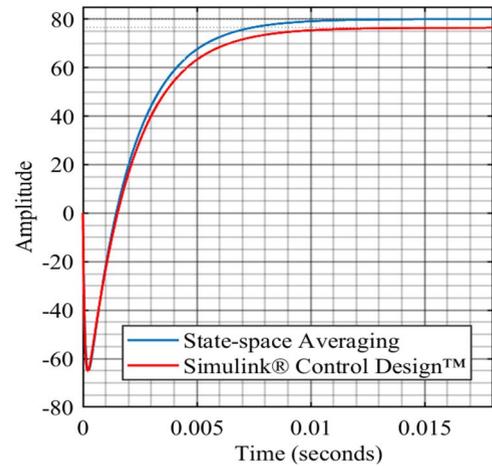
(a) Open-loop Step response.
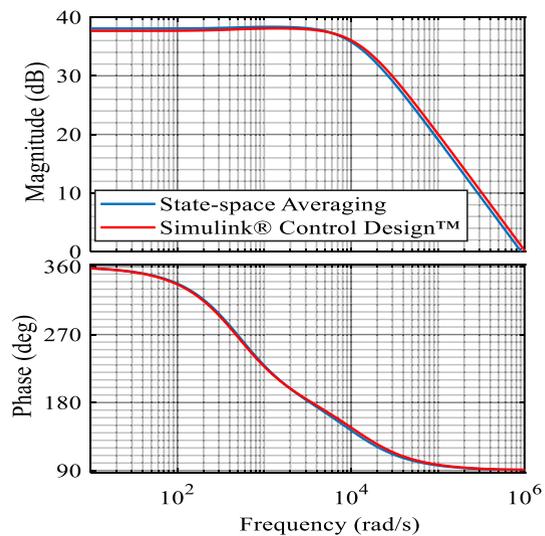
(b) Open-loop Frequency response.

FIGURE 5. Time and frequency responses of derived transfer functions.
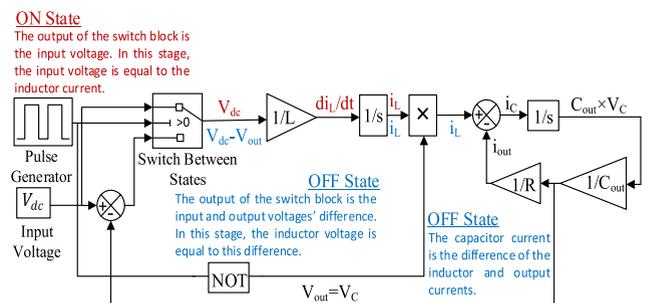
FIGURE 6. The differential equation model of the DBC.

supplies (SMPS) with Left Half Plane-zero (LHPZ). The input voltage, output voltage, load resistance, inductance, and output capacitance all affect the boost converter's double-pole and RHP-zero, further complicating the transfer function. To ensure proper functioning, it is necessary to understand
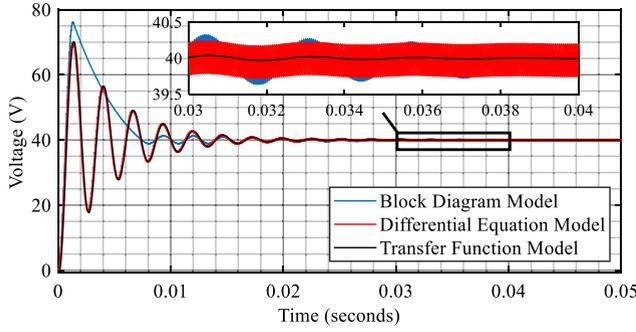
FIGURE 7. Comparison of output voltages for different mathematical models.

TABLE 7. The effects of PI controller parameters on transient response.

Closed-loop Response	Rise Time	Overshoot	Settling Time	Steady-state Error
K_p	Decrease	Increase	Small Change	Decrease
K_i	Decrease	Increase	Increase	Decrease

the transfer function and have a mechanism to stabilize the converter. Plants whose input-output transfer functions have right half plane zeros are described as non-minimum phase systems. RHPZs are the mathematical description of the non-minimum phase systems. Physically, it refers to emergent of undershoot or to the systems goes in the wrong direction initially as impulse or step inputs are applied. Generation of the undershoot can be considered as some amount of time delay due to similar characteristics although it is not exactly time delay in terms of mathematical representation of the control systems. RHPZs have fundamental limits on the robustness on the system such as limitation on the bandwidth which is how fast of a change can be tracked. In this paper, single PI, cascade PI and cascade PI controller-based model reference adaptive controller will be designed and implemented in the control of the proposed DBC. Additionally, their performances will be evaluated regarding transient and steady-state response characteristics.

A. PI CONTROLLER DESIGN

The mathematical model of the plant is appropriately obtained by using both Simulink® Control Design™ and state-space averaging technique to forecast its response and observe its behaviors in both the time and frequency domains. Control systems are planned and executed in this regard to improve critical dynamic properties of the plant, such as stability, response time, steady-state error, and oscillations that make up the transient and steady-state. Because of its features of being simple to design, easily comprehensible, and very understandable, the Proportional-Integral (PI) feedback compensator structure is a commonly used controller. The general effects of each controller parameter proportional gain (K_p) and integral gain (K_i) on a closed-loop system are summarized in Table 7.
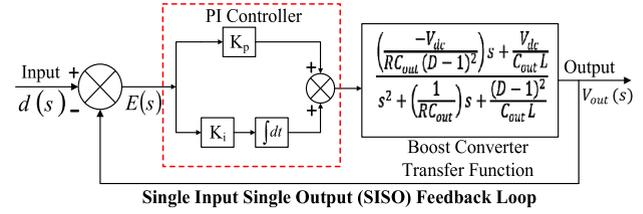
FIGURE 8. The unity feedback structure of the proposed DBC.
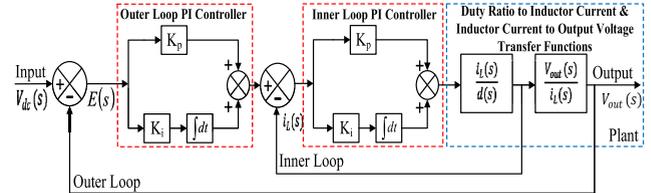
FIGURE 9. The cascade PI controller structure of the proposed DBC.

The unity feedback structure of the proposed DBC is given in Figure 8.

PI controller transfer function of the proposed DCB is given in Eq. (33):

$$G_{PI}(s) = \frac{0.0114s + 2.82}{s} \tag{33}$$

B. CASCADE PI CONTROLLER DESIGN

Cascade control is primarily utilized to ensure rapid disturbance rejection before it spreads to other parts of the plant. As illustrated in the block diagram in Figure 9, the simplest cascade control system has two control loops (inner and outer). The inner loop of the proposed system is the transfer function of duty ratio to inductor current which is derived by using state-space averaging method as:

$$sx(s) = Ax(s) + [(A_1 - A_2)X + (B_1 - B_2)V_{dc}]d(s) \tag{34}$$

$$i_L(s) = Cx(s) + [(C_1 - C_2)X]d(s) \tag{35}$$

$$x(s) = (sI - A)^{-1}[(A_1 - A_2)X + (B_1 - B_2)V_{dc}]d(s) \tag{36}$$

$$i_L(s) = C[(sI - A)^{-1}[(A_1 - A_2)X + (B_1 - B_2)V_{dc}]d(s)] + [(C_1 - C_2)X]d(s) \tag{37}$$

$$\frac{i_L(s)}{d(s)} = C[(sI - A)^{-1}[(A_1 - A_2)X + (B_1 - B_2)V_{dc}] + [(C_1 - C_2)X] \tag{38}$$

$$= \frac{sRC_{out}V_{dc} + 2V_{dc}}{s^2[LRC_{out}(1-D)] + sL(1-D) + R(1-D)^3} \tag{39}$$

$$\frac{i_L(s)}{d(s)} = \frac{0.00176s + 40}{4.4e - 09s^2 + 5e - 05s + 0.025} \tag{40}$$

Inductor current to output voltage transfer function is derived as:

$$\frac{V_{out}(s)}{i_L(s)} = \frac{\frac{V_{out}(s)}{d(s)}}{\frac{i_L(s)}{d(s)}}$$

$$= -\frac{(RV_{dc}\sigma^2 - LV_{dc}s)(R\sigma^3 + Ls\sigma + C_{out}LR\sigma s^2)}{(2V_{dc} + C_{out}RV_{dc}s)(R\sigma^4 + LsV_{dc} + C_{out}LR\sigma^2 s^2)} \tag{41}$$
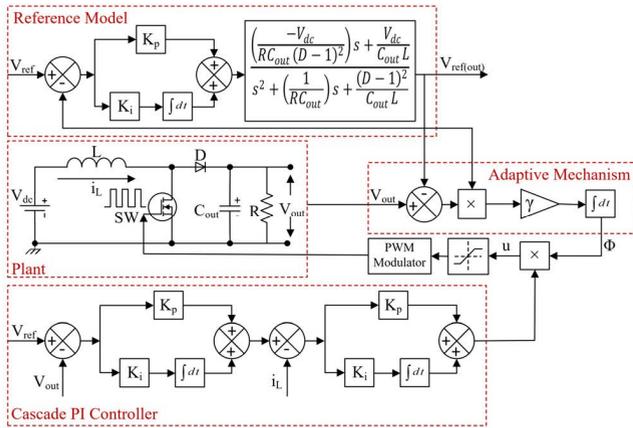
FIGURE 10. The block diagram of proposed cascade PI-based MRAC.

where σ is D − 1.

$$= \frac{-8.8e-12s^3-9.56e-08s^2+0.025}{3.872e-12s^3+1.32e-07s^2+o.oo1022s+0.5}$$

PI controller in the outer loop is the primary controller and it regulates the primary control variable input voltage V_{dc} by setting the set point of the inner loop. PI controller in the inner loop is the secondary controller that ensures local disturbance rejection before it propagates to the inductor current to output voltage transfer function. For the proper functioning of the cascade systems, the inner loop response must be faster than the outer loop. In this application, the inner loop bandwidth is selected 10 times higher than the outer loop bandwidth. Outer and inner loop PI controller transfer functions are given in Eq. 43 and 44, respectively.

$$G_{outer,PI}(s) = \frac{0.15s + 1000}{s} \qquad (42)$$

$$G_{inner,PI}(s) = \frac{0.5s + 5}{s} \qquad (43)$$

C. CASCADE PI-BASED MODEL REFERENCE ADAPTIVE CONTROLLER DESIGN

The control method employed by a controller which adapts to a controlled system with varying or initially uncertain parameters is known as adaptive control. Parameter estimation is the foundation of the adaptive control, which is an important constituent of system identification. In this paper, the model reference adaptive controller (MRAC) is implemented with cascade PI controller. The main components of a MRAC system are the reference model, the adjustment mechanism, and the controller. The proposed cascade PI-based MRAC block diagram is given in Figure 10.

In the proposed control scheme, the adaptation mechanism adjusts the control action based on the error between the plant output V_{out} and the reference model output $V_{ref(out)}$ as:

$$\Phi = (V_{out} - V_{ref(out)})V_{ref(out)}\frac{-\Upsilon T_s z}{z - 1} \qquad (44)$$

TABLE 8. Calculated values of the reference boost converter model.

Parameters and Components	Value
Minimum Load Resistance (Ω)	10
Steady-state Duty Cycle (D)	0.5
Maximum Average Inductor Current (A)	8
Maximum Average Inductor Current Ripple (A)	1.6
Inductor Value (mH)	0.3125
Output Voltage Ripple (V)	1.6
Capacitor Value (μF)	62.5

where Φ, Υ and T_s are adaptation parameter, learning rate and sample time, respectively. The adjusted control signal u is calculated as multiplication of output of the cascade PI controller and adaptation parameter. The desired behavior of the closed-loop system is obtained by using learning rate of 0.04 and sample time of $1/10f_{sw}$ seconds.

D. REFERENCE MODEL DESIGN

The steady state duty cycle of the plant in terms of input-output voltage relationship is represented by

$$\frac{V_{out}}{V_{dc}} = \frac{1}{(1 - D)} \qquad (45)$$

The maximum average inductor current is represented by:

$$I_{L,avg,max} = \frac{V_{out}^2}{R_{out,min}V_{dc}} \qquad (46)$$

The maximum average inductor ripple current is the 20% of the average current that is represented by:

$$\Delta I_L = 0.2 \times I_{L,avg,max} \qquad (47)$$

Inductance value L of the inductor is represented by:

$$L = \frac{V_{in}D}{f_{sw}\Delta I_L} \qquad (48)$$

Capacitor ΔV_C or output voltage ripple ΔV_{out} is the ±2% of the average output voltage is represented by:

$$\Delta V_C = \Delta V_{out} = 0.04 \times V_{out} \qquad (49)$$

Capacitance value C of the capacitor is represented by:

$$C = \frac{V_{in}D}{R_{out,min}f_{sw}\Delta V_C(1 - D)} \qquad (50)$$

The calculated values of the reference boost converter model parameters are given in Table 8.

Transfer functions of the reference model boost converter and PI controller are given in Eq. 52 and 53, respectively.

$$G_{ref,DBC}(s) = \frac{-0.0625s+50}{4.88e-08s^2+7.813e-05s+0.625} \qquad (51)$$

$$G_{ref,PI}(s) = \frac{0.000005s + 7.5}{s} \qquad (52)$$
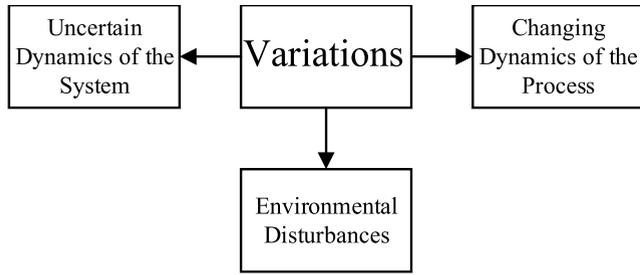
FIGURE 11. The variations in the process dynamics.

FIGURE 12. The block diagram of the MRAC.

E. DESCRITIZATION OF THE DESIGNED CONTROLLERS AND REFERENCE BOOST CONVERTER TRANSFER FUNCTION

The controller in digital control systems is implemented on a digital computer, which means it will only run and have access to measurements at specific and discrete times before commanding the actuators. When a continuous system is converted to a discrete system, information is lost, which might have a detrimental impact on the proposed control system performance. Furthermore, discrete systems introduce delay into the feedback loop, reducing the controller's bandwidth. The bandwidth is an important parameter since it specifies the maximum frequency at which the control system can respond. Considering these difficulties, selecting a proper discretization approach is critical

The zero-order hold (ZOH), first-order hold (FOH), impulse invariant, bilinear (Tustin) approximation, and matched pole-zero technique are some of the most prevalent discretization methods used in control systems. The designed controllers and reference boost converter model is discretized using the bilinear (Tustin's approach) approximation. The most important argument for employing this method is that it produces the best frequency-domain match between continuous-time and discrete systems. The equation employed in the approximation of the z-domain transfer function relating to its continuous form (s-domain) with sample frequency one order of magnitude higher than the switching frequency ($T_s = 1/10f_{sw}$) is given by the following equation:

$$z = e^{sT_s} \approx \frac{1 + sT_s/2}{1 - sT_s/2} \qquad (53)$$

V. STABILITY ANALYSIS OF THE PROPOSED CONTROL SCHEME AND TIME DOMAIN PERFORMANCE COMPARISON

An adaptive controller adapts to variations and adjusts to changes in the process dynamics. In this regard, it must be set up in such a way that one can handle all variations in the system stated in Figure 11.

There are different techniques such as robust controller and gain scheduling developed to deal with uncertainty explicitly. Robust control approach is based on the ground of designing controller with enough stability and performance margin that it works sufficiently well across the entire range of expected
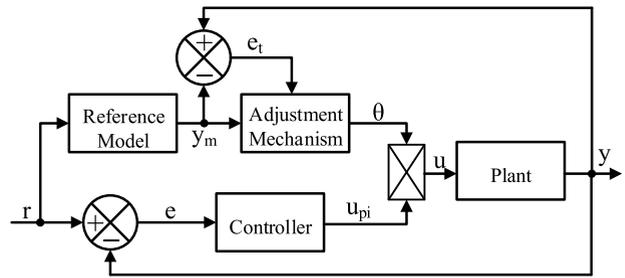
TABLE 9. The PI controller based MRAC parameters.

Name	Parameter
Controller output	u_{pi}
Proportional gain	K_p
Intergral gain	K_i
Sample time	T_s
Error	e
Adaptation parameter	θ
Plant output	y
Reference model output	y_m
Learning rate	γ
Adjusted control signal	u

variations. The problem associated with this approach is that meeting requirements becomes more challenging as the range of uncertainty grows. At this point, gain scheduling approach can be considered as an alternative as it updates controller gains in the event of system state changes. Although gain scheduling works well for large variations, it does not work well for unexpected variations since gain sets and states must be known ahead of time. Adaptive control technique offers an effective alternative to resolve the arising problems associated with the use of both robust and gain scheduling approaches. The block diagram of the MRAC is given in Figure 12.

Parameters of the MRAC shown in Figure 12. With their names are given in Table 9.

The control equation of the MRAC is given as:

$$u_{pi}(k) = \left[K_p + K_i \frac{T_s z}{z - 1} \right] e(k) \qquad (54)$$

The adaptation mechanism whose function is control action adjustment based on the error between the plant output and the reference model output. The adaptation parameter equation is given as:

$$\theta = (y - y_m) y_m \frac{-\gamma T_s z}{z - 1} \qquad (55)$$

Designing principle of the MRAC by using MIT rule requires identification of the reference model, the controller structure, and tuning gains for the adjustment mechanism
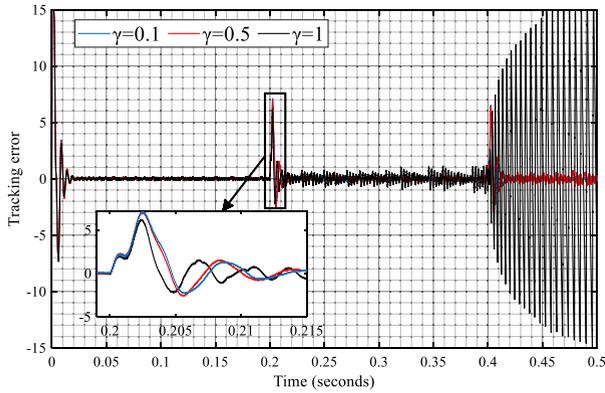
FIGURE 13. Tracking error of the system for varying learning rates.

FIGURE 14. Converging trajectories of the adaptation parameter for varying learning rates.

FIGURE 15. The plant output voltages for varying learning rates.

TABLE 10. Step response characteristics comparison of the controllers.

Step Reponse Characteristics	Single PI Control	Cascade PI Control	Cascade PI-based MRAC
Rise Time	5.9e-04	0.0012	0.0014
Settling Time	0.0079	0.0064	0.00145
Settling Minimum	33.69	37.564	39.7
Settling Maximum	40.164	44.697	41.485
Overshoot (%)	0.41	11.7425	3.7125
Undershoot (%)	3.16	0.1	0
Peak	40.164	44.697	41.485
Peak Time	0.001	0.0028	0.0025

[53], [54]. The formulations process of the MRAC begins with definition of the tracking error e_t given as:

$$e_t = y - y_m \qquad (56)$$

A typical cost function of θ, $J(\theta)$, is formed by using the tracking error e_t as the following [55]:

$$J(\theta) = \frac{1}{2}e_t^2(\theta) \qquad (57)$$

The MIT rule describes the relationship between the change in theta and the cost function [56], [57]. To determine how to update the parameter theta, an equation for the change in theta must be created [58]. Assumed that the change in $J(\theta)$ is proportional to the change in θ, the MIT sensitivity derivative equations is generated as [59]:

$$\frac{d\theta}{dt} = -\gamma \frac{\delta J(\theta)}{\delta \theta} = -\gamma e_t \frac{\delta e_t}{\delta \theta} \qquad (58)$$

The tracking error e_t of the system regulated by implementation of the proposed Cascade PI controller based MRAC scheme under varying learning rates ($\gamma = 0.1, 0.5$ *and* 1) for reference voltages of 30 V, 40 V and 50 V applied at 0, 0.2 and 0.4 seconds, respectively is given in Figure 13. The tracking error e_t shows a tendency to become zero with a quick pace with the increasing learning rates.

The converging trajectories of the adaptation parameter θ for varying values of the learning rate γ when a step change from 30 V to 40 V is applied at 0.2 seconds as a controlled input to the system is shown in Figure 14. Angle of inclination for the adaptation parameter decreases and consequently convergence of the adaptation parameter θ increases for larger values of γ.

Actual voltage outputs of the system in response to the step input voltages changing from 30 V to 40 V at 0.2 seconds and 40 V to 50 V at 0.4 seconds is applied are given in Figure 15.

For larger γ values, the parameters' convergence increases. This demonstrates that the controller is functional and that the equations have been correctly implemented. Larger values of γ, on the other hand, cause the control transients to oscillate as it can be seen in Figures 13, 14 and 15. The results

of time domain performance analysis of the investigated and proposed algorithms are given in Table 10.

Achieving a better tracking performance is possible with higher values of γ, however it leads to increase in the overshoot and choosing the best attainable value of the learning rate regarding requirements for the purpose of coherent between performance parameters of the process such as rise time, overshoot and settling time.
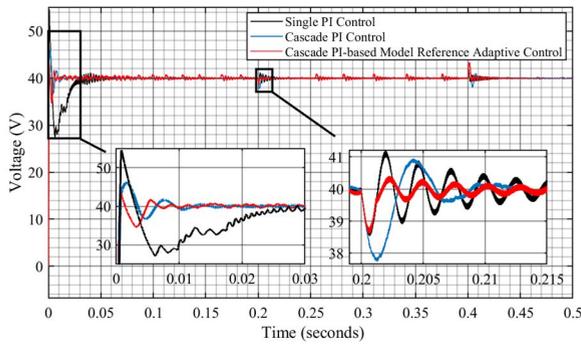
FIGURE 16. Comparison of control techniques under varying loads.
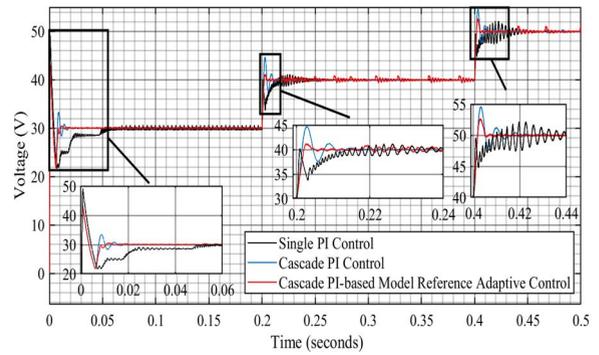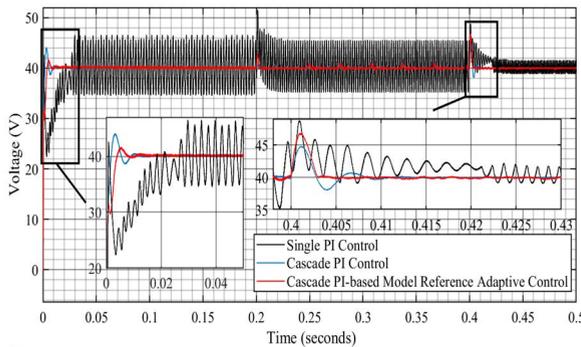
FIGURE 17. Comparison of control techniques under varying loads and different input voltages.

VI. SIMULATION AND EXPERIMENTAL RESULTS

Verification and validation of the proposed Cascade PI-based MRAC compared to the Single PI and Cascade PI controllers have been presented to illustrate the proposed controller scheme efficiency by considering the major concerns such as complex dynamics of the DBC due to NMP behavior and non-linearity. Additionally, the main issues in control system designing, e.g., uncertainty, intended simplicity, stochastic occurrences, and process variability have been considered. Accordingly, the performance of the proposed control has been evaluated by investigating three possible cases: (i) varying resistive loads, (ii) varying input voltages and (iii) varying reference voltages by using MATLAB® and Simulink®.

Figure 16. shows the DBC output voltages with resistive loads varying from 10 to 20 Ω (25% variation fo the nominal value). The proposed Cascade PI-based MRAC strategy shows enhanced transient response with less oscillation.

Figure 17. shows the DBC output voltage waveforms in the presence of both variable resistive load and different input voltages varying between 15 to 25 V (25% variation of the nominal value). Detrimental effect on the output voltage of single PI controlled DBC has been particularly clear is a result of implementing the load and input voltage variations together The Cascade PI-based Reference Model Adaptive control strategy shows enhanced transient response with less oscillation compared to other control techniques.

Figure 18. shows the DBC output voltage waveforms with reference voltages varying from 30 to 50 V (25% varia- tion of the nominal value). In comparison to other control

FIGURE 18. Comparison of control techniques for varying reference voltages.
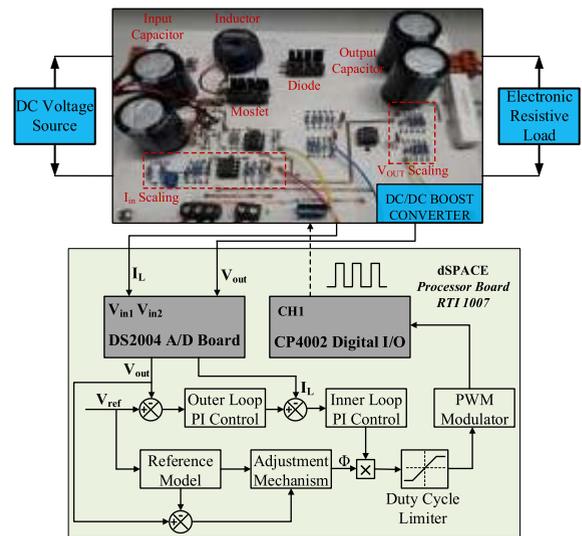
FIGURE 19. Experimental set-up configuration for testing the proposed cascade PI-based MRAC.

systems, the Cascade PI-based Reference Model Adaptive control strategy shows improved transient response with less oscillation.

Figure 19. shows the block diagram of the experi- mental set-up configuration for evaluating performance of the proposed Cascade PI-based Model Reference Adaptive Controller. The DC-DC boost converter, the electronic resis- tive load for continuous DC voltage output, the DC voltage source and the dSPACE real-time Interface (RTI) hardware- in-the-loop (HIL) control panels (RTI 1007 processor board, DS2004 High-Speed A/D, and CP4002 Timing and Digital I/O boards) comprise up the overall system.

Test bench of the experiment is given in Figure 20. The designed boost converter is connected with a 300 W pro- grammable DC power supply (Tenma-72-2940 with 60 V maximum output voltage and 5 A maximum out- put current) which is used for DC input voltage. Additionally, an adjustable bench power supply with 3 out- puts (AL991A-48 W power rating, −15 minimum output voltage and +15 maximum output voltage) is utilized to run the converter and a DC electronic load (3362F High Voltage DC Electronic Load 500V,60A,1800W) is used for setting the output load resistance. The proposed Cascade PI-based
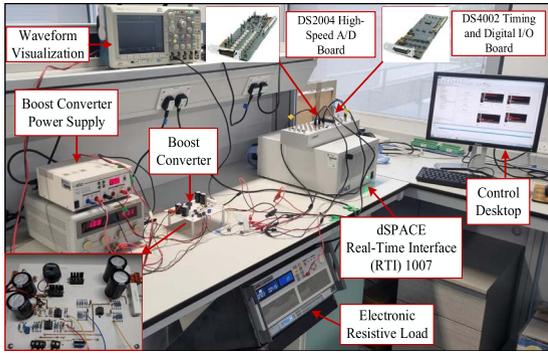
FIGURE 20. Test bench of the overall system.
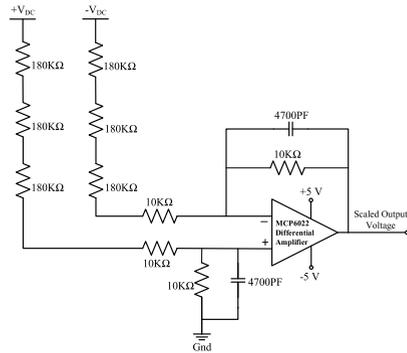
(a) Output voltage scaling circuit.
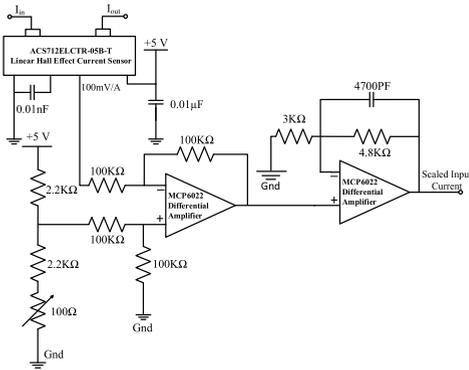
(b) Inductor current scaling circuit.

FIGURE 21. Scaling circuits of output voltage and inductor current for providing their integration with dSPACE control panel.

Model Reference Adaptive Control, Single PI and Cascade PI Control methods developed by using MATLAB/Simulink was implemented via dSPACE rapid control prototyping. The RTI block of the Modular Hardware/DS2004 High-speed A/D was used to convert the measured inductor current I_L and output voltage V_{out} as shown in Figure 19.

The converted I_L and V_{out} were then implemented in the designed control techniques. Since the operating input voltage limits for DS2004 High-Speed A/D Board is specified as ranging from -10 V to $+10$ V, actual input current and output voltage are scaled down to meet the requirement. V_{out} and I_L were scaled down by a constant factor of 56 and 2.6, respectively. The scaling circuits are given in Figure 21.

The PWM signal for running the boost converter was generated using a regulated duty cycle in Simulink to attain the desired terminal voltage. dSPACE MATLAB/Simulink
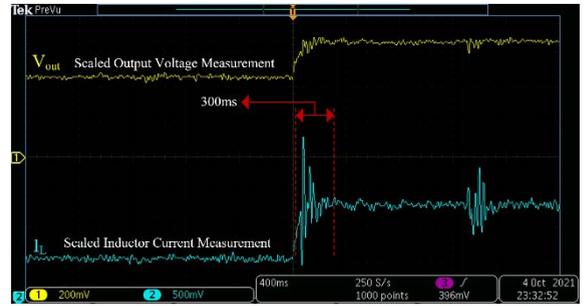
FIGURE 22. Output voltage and inductor current waveforms of single PI controlled DBC.
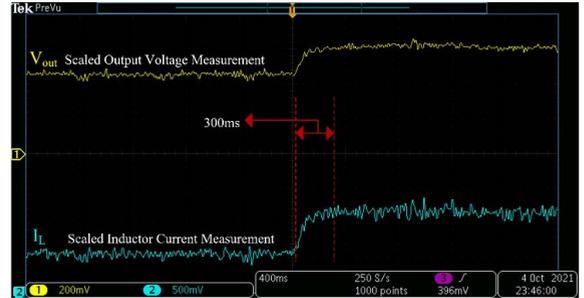
FIGURE 23. Output voltage and inductor current waveforms of cascade PI controlled DBC.
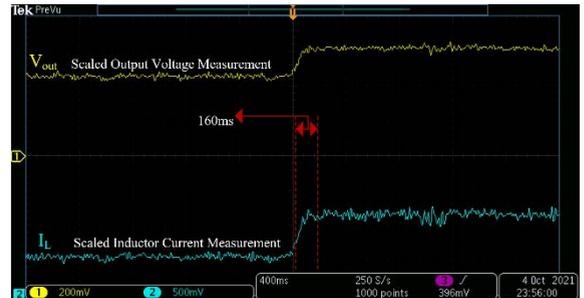
FIGURE 24. Output voltage and inductor current waveforms of the DBC controlled with proposed cascade PI-based MRAC.

PC-based simulation platform Modular Hardware/DS4002 Timing and Digital I/O Board was used to implement the generated digital PWM signal.

Scaled output voltage and inductor current waveforms during step change of the load (reference voltage change from 25 V to 40 V) for the designed single PI controlled DBC is given in Figure 22.

Scaled output voltage and inductor current waveforms during step change of the load (reference voltage change from 25 V to 40 V) for the designed cascade PI controlled DBC is given in Figure 23.

Scaled output voltage and inductor current waveforms during step change of the load (reference voltage change from 25 V to 40 V) for the designed DBC controlled by cascade PI-based reference model adaptive control technique is given in Figure 24.

Application of the single PI controller for the boost converter refers to voltage-mode control which also known as duty-cycle control. This control scheme uses a single loop to adjust the duty cycle in direct response to changes in output voltage. Because of the boost converter's inherent

RHPZ, a voltage-mode controlled boost converter operating in continuous conduction mode is more difficult to stabilise and it means to have poor transient response with disturbance occurrence as shown in Figure 22.

The cascade PI control of the boost converter refers to current-mode control that contains two loops (an inner current loop and outer voltage loop) with inner and outer PI controllers. The cascade control system performs substantially better in rejecting disturbance, although the set-point tracking performances are nearly comparable, based on the two response plots given in Figure 17 and 18. Moreover, even if the RHPZ is at a low frequency, compensation for cascade PI controlled boost converters is significantly easier than compensation for single PI controlled boost converters. Since the crossover frequency has no minimum requirement in cascade control, the system can be stabilized regardless of the RHPZ frequency. The inner current loop eliminates the filter's ringing frequency, and good performance is attained even with a low voltage feedback loop crossover frequency.

The experimental results are consistent with the simulation outcomes. The suggested cascade PI-based reference model adaptive control technique compared to other two methods improved transient response with considerable disturbance rejection, according to both experimental and analytical results.

VII. CONCLUSION

A DC-DC boost converter with Cascade PI Controller-Based Robust Model Reference Adaptive Control (MRAC) is presented in this paper. The boost converter's non-minimum phase behaviour owing to right half plane zero is a challenge, and its non-linear dynamics hinder the control process while in continuous conduction mode (CCM). By combining aspects of a cascade PI control loop with MRAC characteristics, the suggested control strategy effectively overcame complexities and challenges. Fundamental objective of integrating MRAC to the cascade PI controlled boost converter was to maintain consistent performance in the presence of uncertainty, variations in plant parameters and non-linear dynamics.

Using MATLAB/Simulink, the comparative analysis with single PI and cascade PI controllers, the validity of the proposed control system's ability to track the desired signals and regulate the plant process variables in the most beneficial and optimised way without delay and overshoot is verified.

Furthermore, the suggested control scheme's performance as well as single and cascade PI controllers is experimentally evaluated using MATLAB/Simulink/Stateflow on the dSPACE RTI 1007 processor, DS2004 High-Speed A/D, and CP4002 Timing and Digital I/O boards. The experimental and analytical results show that the proposed control method increased tracking speed by two times while also providing better disturbance rejection.

COMPETING INTERESTS

The authors declare that they have no competing interests.

REFERENCES

[1] R. Ayop and C. W. Tan, "A comprehensive review on photovoltaic emulator," *Renew. Sustain. Energy Rev.*, vol. 80, pp. 430–452, Dec. 2017.

[2] S. Seyam, I. Dincer, and M. Agelin-Chaab, "Development of a clean power plant integrated with a solar farm for a sustainable community," *Energy Convers. Manage.*, vol. 225, Dec. 2020, Art. no. 113434.

[3] S. Paul, T. Dey, P. Saha, S. Dey, and R. Sen, "Review on the development scenario of renewable energy in different country," in *Proc. Innov. Energy Manage. Renew. Resour. (IEMRE)*, vol. 2, Feb. 2021, pp. 1–2.

[4] T. W. J. Twidell, *Renewable Energy Resources*, 3rd ed. New York, NY, USA: Routledge, 2015.

[5] N. L. Panwar, S. C. Kaushik, and S. Kothari, "Role of renewable energy sources in environmental protection: A review," *Renew. Sustain. Energy Rev.*, vol. 15, no. 3, pp. 1513–1524, Apr. 2011.

[6] I. Jawad Hashim, "A new renewable energy index," in *Proc. 6th Int. Conf. Renew. Energy, Gener. Appl. (ICREGA)*, Feb. 2021, pp. 229–232.

[7] E. I. Carroll, "Power electronics for very high power applications," in *Proc. 7th Int. Conf. Power Electron. Variable Speed Drives ABB Rev.*, no. 2, 1999, pp. 4–11.

[8] S. Natarajan, T. Sudhakar Babu, K. Balasubramanian, U. Subramaniam, and D. J. Almakhles, "A state-of-the-art review on conducted electromagnetic interference in non-isolated DC to DC converters," *IEEE Access*, vol. 8, pp. 2564–2577, 2020.

[9] E. M. G. Rodrigues, R. Godina, and E. Pouresmaeil, "Industrial applications of power electronics," *Electronics*, vol. 9, no. 9, pp. 1–5, 2020.

[10] A. Rufer, "Today's and tomorrow's meaning of power electronics within the grid interconnection keywords," in *Proc. Eur. Conf. Power Electron. Appl.*, 2007, pp. 1–11.

[11] P. K. Steimer, "Enabled by high power electronics—Energy efficiency, renewables and smart grids," in *Proc. Int. Power Electron. Conf. (ECCE ASIA, IPEC)*, Jun. 2010, pp. 11–15.

[12] A. Q. Huang, S. Bhattacharya, M. Baran, B. Chen, and C. Han, "Active power management of electric power system using emerging power electronics technology," in *Proc. IEEE Power Eng. Soc. Gen. Meeting (PES)*, Jun. 2007, pp. 1–7.

[13] F. Blaabjerg, K. Ma, and D. Zhou, "Power electronics and reliability in renewable energy systems," in *Proc. IEEE Int. Symp. Ind. Electron.*, May 2012, pp. 19–30.

[14] P. Singh, R. Singh, R. Sharma, and P. Agrawal, "Reliability measures for switched-mode power supplies (SMPS) with redundant fly back transformer," in *Proc. Int. Conf. Micro-Electron. Telecommun. Eng. (ICMETE)*, Sep. 2016, pp. 587–593.

[15] A. Rahnamaee, J. Milimonfared, K. Malekian, and M. Abroushan, "Reliability consideration for a high power zero-voltage-switching flyback power supply," in *Proc. 13th Int. Power Electron. Motion Control Conf. (EPE-PEMC)*, 2008, pp. 373–379.

[16] J. Popović-Gerber, J. A. Oliver, N. Cordero, T. Harder, J. A. Cobos, M. Hayes, S. C. O'Mathuna, and E. Prem, "Power electronics enabling efficient energy usage: Energy savings potential and technological challenges," *IEEE Trans. Power Electron.*, vol. 27, no. 5, pp. 2338–2353, May 2012.

[17] Q. Yin, J. Gan, T. Chen, W. Shi, X. Liu, and Z. Chang, "Research on the flyback switch power supply based on the primary feedback and the valley control," in *Proc. IEEE 9th Joint Int. Inf. Technol. Artif. Intell. Conf. (ITAIC)*, Dec. 2020, pp. 1312–1315.

[18] B. M. Hasanien and K. F. A. Sayed, "Current source ZCS PFM DC-DC converter for magnetron power supply," in *Proc. 12th Int. Middle-East Power Syst. Conf.*, Mar. 2008, pp. 464–469.

[19] J.-H. Wu, W. He, J. Li, and X. Liu, "GaN high frequency small switching power module," in *Proc. IEEE 2nd Int. Conf. Circuits Syst. (ICCS)*, Dec. 2020, pp. 101–104.

[20] D. Kumar, Amarnath, R. Jain, and R. K. Singh, "Comparison of non-isolated boost converter & isolated flyback converter for PV application," in *Proc. Int. Conf. Innov. Control. Commun. Inf. Syst. (ICICCI)*, 2019, pp. 1–7.

[21] B. M. Reddy and P. Samuel, "A comparative analysis of non-isolated bi-directional DC-DC converters," in *Proc. IEEE 1st Int. Conf. Power Electron., Intell. Control Energy Syst. (ICPEICES)*, Jul. 2016, pp. 1–6.

[22] A. Alassi, A. Al-Aswad, A. Gastli, L. B. Brahim, and A. Massoud, "Assessment of isolated and non-isolated DC-DC converters for medium-voltage PV applications," in *Proc. 9th IEEE-GCC Conf. Exhib. (GCCCE)*, May 2017, pp. 1–6.

[23] B. M. Hasaneen and A. A. E. Mohammed, "Design and simulation of DC/DC boost converter," in *Proc. 12th Int. Middle-East Power Syst. Conf. (MEPCON)*, Mar. 2008, pp. 335–340.

[24] S. Banerjee, A. Ghosh, and S. Padmanaban, "Modeling and analysis of complex dynamics for dSPACE controlled closed-loop DC-DC boost converter," *Int. Trans. Electr. Energy Syst.*, vol. 29, no. 4, pp. 1–17, 2019.

[25] H. Li, X. Liu, and J. Lu, "Research on linear active disturbance rejection control in DC/DC boost converter," *Electronics*, vol. 8, no. 11, p. 1249, Oct. 2019.

[26] S. Ahmad and A. Ali, "Active disturbance rejection control of DC–DC boost converter: A review with modifications for improved performance," *IET Power Electron.*, vol. 12, no. 8, pp. 2095–2107, Jul. 2019.

[27] Y. Zhang, H. Liu, J. Li, M. Sumner, and C. Xia, "DC-DC boost converter with a wide input range and high voltage gain for fuel cell vehicles," *IEEE Trans. Power Electron.*, vol. 34, no. 5, pp. 4100–4111, May 2019.

[28] A. Özdemir and Z. Erdem, "Double-loop PI controller design of the DC-DC boost converter with a proposed approach for calculation of the controller parameters," *Proc. Inst. Mech. Eng. I, J. Syst. Control Eng.*, vol. 232, no. 2, pp. 137–148, Feb. 2018.

[29] T. Kobaku, R. Jeyasenthil, S. Sahoo, R. Ramchand, and T. Dragicevic, "Quantitative feedback design-based robust PID control of voltage mode controlled DC-DC boost converter," *IEEE Trans. Circuits Syst. II, Exp. Briefs*, vol. 68, no. 1, pp. 286–290, Jan. 2021.

[30] Q. Xu, N. Vafamand, L. Chen, T. Dragicevic, L. Xie, and F. Blaabjerg, "Review on advanced control technologies for bidirectional DC/DC converters in DC microgrids," *IEEE J. Emerg. Sel. Topics Power Electron.*, vol. 9, no. 2, pp. 1205–1221, Apr. 2021.

[31] A. R. Nikhar, S. M. Apte, and R. Somalwar, "Review of various control techniques for DC-DC interleaved boost converters," in *Proc. Int. Conf. Global Trends Signal Process., Inf. Comput. Commun. (ICGTSPICC)*, Dec. 2016, pp. 432–437.

[32] M. F. Adnan, M. A. M. Oninda, M. M. Nishat, and N. Islam, "Design and simulation of a DC–DC boost converter with PID controller for enhanced performance," *Int. J. Eng. Res.*, vol. 6, no. 9, pp. 27–32, Sep. 2017.

[33] B. Hekimoglu, S. Ekinci, and S. Kaya, "Optimal PID controller design of DC-DC buck converter using whale optimization algorithm," in *Proc. Int. Conf. Artif. Intell. Data Process. (IDAP)*, Sep. 2018, pp. 1–6.

[34] F. Mumtaz, N. Z. Yahaya, S. T. Meraj, B. Singh, R. Kannan, and O. Ibrahim, "Sliding mode control and chattering: The concept," *Ain Shams Eng. J.*, vol. 12, no. 4, pp. 3747–3763, 2021.

[35] V. Utkin, A. Poznyak, Y. Orlov, and A. Polyakov, "Conventional and high order sliding mode control," *J. Franklin Inst.*, vol. 357, no. 15, pp. 10244–10261, Oct. 2020.

[36] H. Fatoorehchi and S. A. Ghorbanian, "Sliding mode control for heartbeat electrocardiogram tracking problem," *J. Chem. Petroleum Eng.*, vol. 53, no. 2, pp. 265–272, 2019.

[37] F. M. Zaihidee, S. Mekhilef, and M. Mubin, "Robust speed control of PMSM using sliding mode control (SMC)—A review," *Energies*, vol. 12, no. 9, p. 1669, May 2019.

[38] M. Augustine, "Sliding mode control and chattering: The concept," Mar. 2019.

[39] Q. Wei, B. Wu, D. Xu, and N. R. Zargari, "Model predictive control of capacitor voltage balancing for cascaded modular DC–DC converters," *IEEE Trans. Power Electron.*, vol. 32, no. 1, pp. 752–761, Jan. 2017.

[40] F. An, W. Song, K. Yang, N. Hou, and J. Ma, "Improved dynamic performance of dual active bridge DC–DC converters using MPC scheme," *IET Power Electron.*, vol. 11, no. 11, pp. 1756–1765, Sep. 2018.

[41] E. Irmak and N. Güler, "A model predictive control-based hybrid MPPT method for boost converters," *Int. J. Electron.*, vol. 107, no. 1, pp. 1–16, Jan. 2020.

[42] O. Ibrahim, N. Z. Yahaya, and N. Saad, "State-space modelling and digital controller design for DC-DC converter," *Telkomnika*, vol. 14, no. 2, pp. 497–506, 2016.

[43] S. Tahir, J. Wang, M. Baloch, and G. Kaloi, "Digital control techniques based on voltage source inverters in renewable energy applications: A review," *Electronics*, vol. 7, no. 2, p. 18, Feb. 2018.

[44] J. Freytes, G. Bergna, J. Are Suul, S. D'Arco, H. Saad, and X. Guillaud, "State-space modelling with steady-state time invariant representation of energy based controllers for modular multilevel converters," in *Proc. IEEE Manchester PowerTech*, Jun. 2017, vol. 2, no. 2, pp. 1–7.

[45] P. Azer and A. Emadi, "Generalized state space average model for multi-phase interleaved buck, boost and buck-boost DC-DC converters: Transient, steady-state and switching dynamics," *IEEE Access*, vol. 8, pp. 77735–77745, 2020.

[46] Q. A. Tarbosh, O. Aydogdu, N. Farah, M. H. N. Talib, A. Salh, N. Cankaya, F. A. Omar, and A. Durdu, "Review and investigation of simplified rules fuzzy logic speed controller of high performance induction motor drives," *IEEE Access*, vol. 8, pp. 49377–49394, 2020.

[47] R. Araria, A. Berkani, K. Negadi, F. Marignetti, and M. Boudiaf, "Performance analysis of DC-DC converter and DTC based fuzzy logic control for power management in electric vehicle application," *J. Européen des Systèmes Automatisés*, vol. 53, no. 1, pp. 1–9, Feb. 2020.

[48] M. A. Soliman, H. M. Hasanien, H. Z. Azazi, E. E. El-Kholy, and S. A. Mahmoud, "An adaptive fuzzy logic control strategy for performance enhancement of a grid-connected PMSG-based wind turbine," *IEEE Trans. Ind. Informat.*, vol. 15, no. 6, pp. 3163–3173, Jun. 2019.

[49] N. Santos, J. F. Silva, and V. Soares, "Control of single-phase electrolytic capacitor-less isolated converter for DC low voltage residential networks," *Electronics*, vol. 9, no. 9, pp. 1–19, 2020.

[50] K. Yang, G. Q. Wu, and X. D. Zhang, "The control technology of BUCK converter," *Appl. Mech. Mater.*, vol. 150, pp. 240–244, Jan. 2012.

[51] D. Rowell. (Oct. 2002). *State-Space Representation of LTI Systems*. [Online]. Available: http://web.mit.edu/2.14/www/Handouts/StateSpace.pdf

[52] G. Herbst, "A building-block approach to state-space modeling of DC-DC converter systems," *J. Multidisciplinary Sci. J.*, vol. 2, no. 3, pp. 247–267, 2019.

[53] S. Coman, C. Boldisor, and C. Ciusdel, "Combining the MIT and Lyapunov stability adaptive methods for second order systems," in *Proc. 14th Int. Conf. Develop. Appl. Syst. (DAS)*, May 2018, pp. 31–37.

[54] M. Pravika, J. Jacob, and K. P. Joseph, "Design of model reference adaptive–PID controller for automated portable duodopa pump in Parkinson's disease patients," *Biomed. Signal Process. Control*, vol. 68, Jul. 2021, Art. no. 102590.

[55] J. Rothe, J. Zevering, M. Strohmeier, and S. Montenegro, "A modified model reference adaptive controller (M-MRAC) using an updated MIT-rule for the altitude of a UAV," *Electronics*, vol. 9, no. 7, pp. 1–15, 2020.

[56] D. Gezer, Y. Taşçıoğlu, and K. Çelebioğlu, "Frequency containment control of hydropower plants using different adaptive methods," *Energies*, vol. 14, no. 8, p. 2082, Apr. 2021.

[57] M. Swathi and P. Ramesh, "Modeling and analysis of model reference adaptive control by using MIT and modified MIT rule for speed control of DC motor," in *Proc. IEEE 7th Int. Adv. Comput. Conf. (IACC)*, Jan. 2017, pp. 482–486.

[58] M. I. Mosaad, "Model reference adaptive control of STATCOM for grid integration of wind energy systems," *IET Electr. Power Appl.*, vol. 12, no. 5, pp. 605–613, May 2018.

[59] W. Netto, R. Lakhani, and S. M. Sundaram, "Design and performance comparison of different adaptive control schemes for pitch angle control in a twin-rotor-MIMO-system," *Int. J. Electr. Comput. Eng.*, vol. 9, no. 5, pp. 4114–4129, 2019.

CAGFER YANARATES was born in April 1986. He received the M.Sc. degree in power engineering and sustainable energy FHEQ7 Taught Masters/PGDip/PGCert from Swansea University, in 2017, where he is currently pursuing the Ph.D. degree in electrical and electronic engineering. He is mainly engaged in applications of power electronics converters in photovoltaics systems and their control.

ZHONGFU ZHOU received the Ph.D. degree from the University of Sussex, Brighton, U.K., in 2004. He joined the College of Engineering, Swansea University, in 2004, as a Research Officer and was promoted to a Lecturer in power electronics, in July 2016. His research interests include active rectifier, active power filter, and power electronics applications for renewable energy systems and automotive. He had been a member of the International Electrotechnical Commission (IEC), where he had advised on the international standard (IEC TS 62600-30) on electrical power quality requirements for wave, tidal, and other water current energy converters.

· · ·